Supplemental Information

Small RNAs and Hfq capture unfolded RNA target sites during transcription

Margaret L. Rodgers, Brett O'Brien, and Sarah A. Woodson

Supplemental Figures

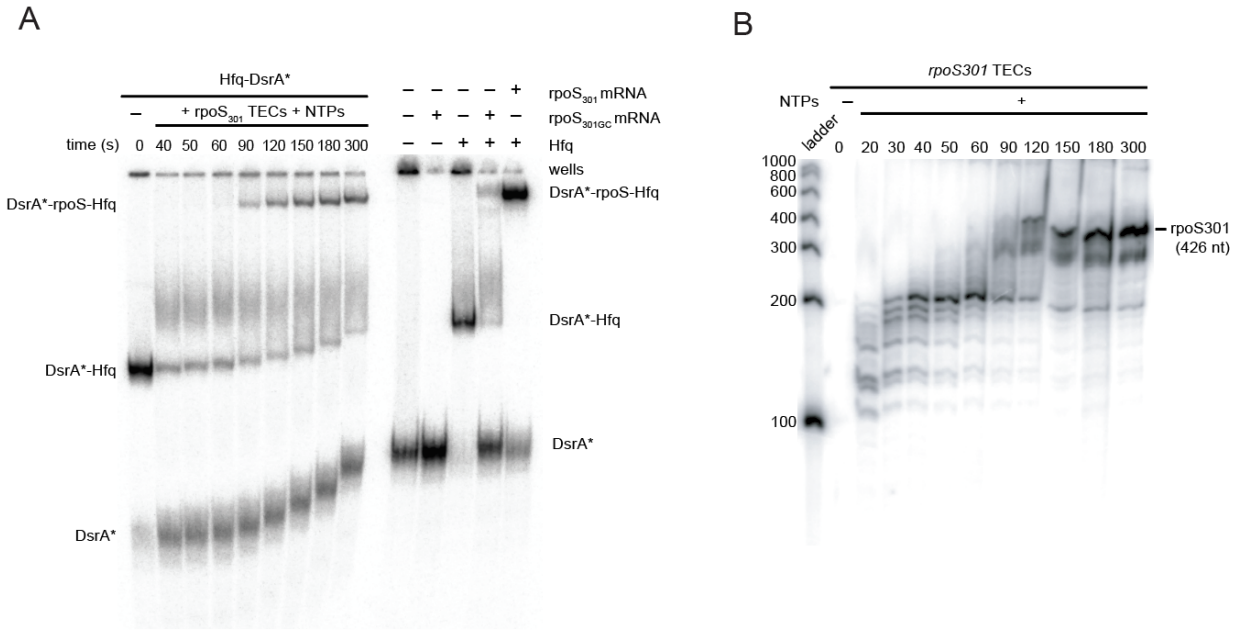

Supplemental Figure S1. Hfq-DsrA form stable ternary complexes with nascent *rpoS* mRNA during transcription. Related to Figure 1.

A) Unlabeled T7 RNA polymerase TECs stalled on a template encoding *rpoS*301 RNA were restarted in the presence of 20 μM NTPs and trace ^{32}P-labeled DsrA•Hfq to monitor association of Hfq-DsrA with *rpoS* mRNAs during and after transcription. Samples were loaded onto a native 8% PAGE at 0 – 300 s after transcription restart. The gel was running continuously during the experiment, so lanes on the right were loaded later than those on the left. Left, a super-shift corresponding to the DsrA•*rpoS*•Hfq ternary complex is observed after 90 s. We only resolve ternary complexes with full-length *rpoS301* because nascent transcripts tethered to T7 RNA polymerase remain in the wells of the gel. Right, binding to refolded, full-length *rpoS*301 RNA (60 min, RT). DsrA-Hfq can associate to form a complex with full-length wild type *rpoS301* mRNA but forms less complex with *rpoS301$_{GC}$* mRNAs containing a GC-clamp mutation as previously reported [1]. DsrA binding is only observed in the presence of Hfq. Excess unlabeled *rpoS301$_{GC}$* mRNA competes Hfq away from DsrA, increasing the amount of free DsrA in the second to last lane.

B) Single round transcription kinetics for *rpoS301* mRNA under the same transcription conditions as in panel A. Transcripts were resolved by denaturing 6% PAGE. Ladder, radiolabeled Riboruler Low Range (Thermo). Full-length *rpoS301* mRNA is first observed at 90 s, corresponding to the time when DsrA-Hfq first associates with *rpoS* mRNA during transcription.

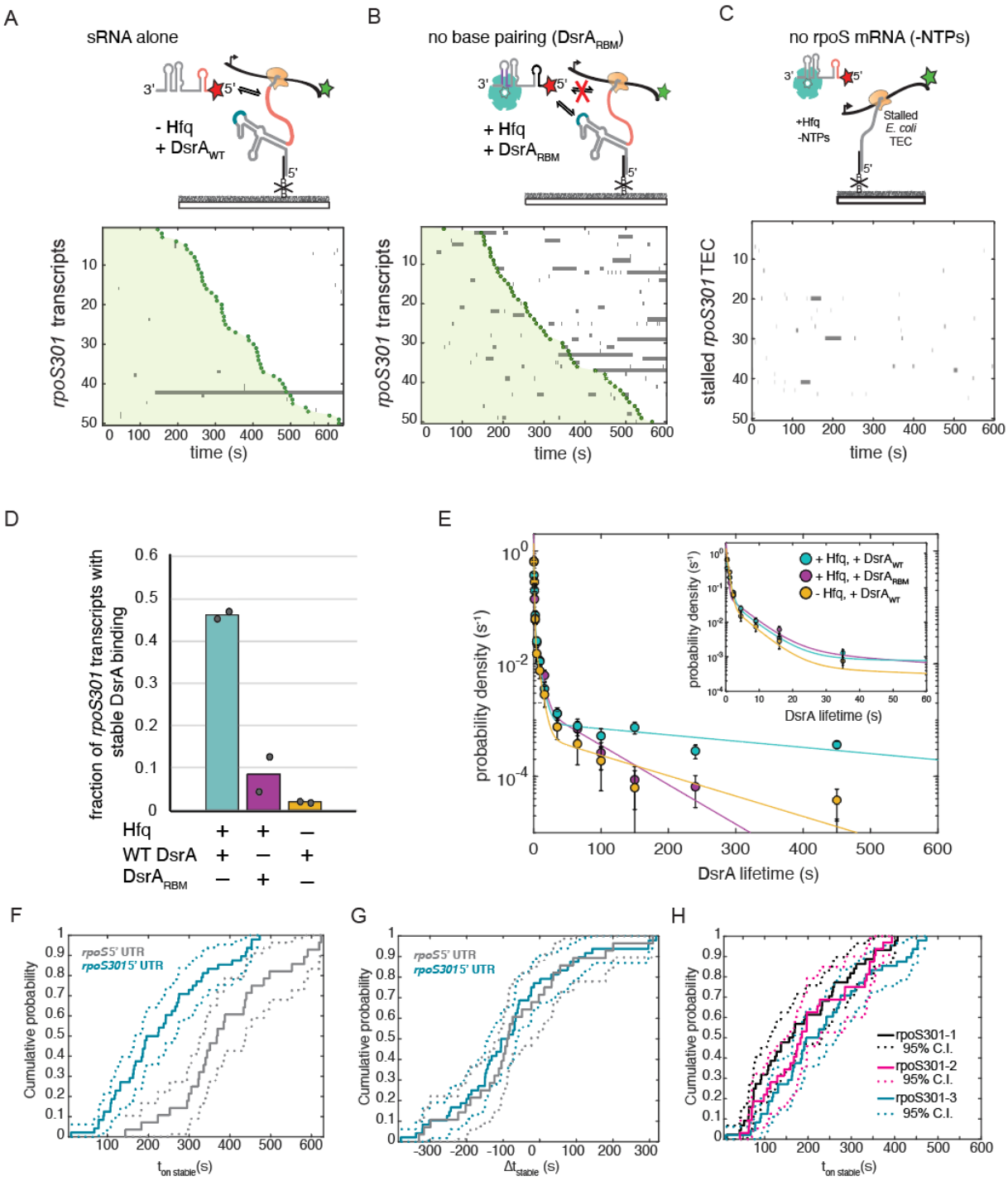

Supplemental Figure S2. Stable Hfq•DsrA targeting depends on Hfq, base pairing, and *rpoS* synthesis. Related to Figure 1, 2.

A) Rastergram of DsrA-Cy5 association with *rpoS301* transcripts in the absence of Hfq, showing little stable binding. Colored as in Fig. 1.

B) Rastergram of non-complementary Hfq•DsrA$_{RBM}$-Cy5 binding to *rpoS301* transcripts. There were fewer stable complexes compared to WT DsrA, in agreement with earlier results (Soper et al., 2011). The presence of a few stable complexes (> 100 s) may indicate residual base-pairing

between $DsrA_{RBM}$ and other regions of the *rpoS*$_{301}$ mRNA or may indicate a low probability of long-lived interactions between Hfq•$DsrA_{RBM}$ and the *rpoS*$_{301}$AAN motif in absence of sRNA-mRNA base pairing.

C) Rastergram of DsrA-Cy5 binding to *rpoS301* stalled TECs in the absence of NTPs. The lack of stable binding indicates that these events likely represent interactions between Hfq-DsrA and nascent *rpoS301* transcripts as opposed to interactions with RNAP or the DNA template. Colored as in Fig. 1.

D) Fraction of immobilized *rpoS301* transcripts that are stably bound by DsrA at some point during the 10 min movie for the components shown. The fractions from two replicate experiments are shown as scatter points and the bar indicates the mean. Details of the number of molecules for each experiment and replicates can be found in Table S2.

E) Probability density histogram with overlayed maximum likelihood triple exponential fit illustrating the distribution of DsrA lifetimes for different conditions. The amplitude of the longest characteristic lifetime among all binding events was diminished in the absence of Hfq or by mutations in DsrA that disrupt base pairing with rpoS mRNA. Equations for fitting can be found in Star Methods. Fit parameters and errors are outlined in Table S1.

F and G) Cumulative probability density plots as in Figure 2B and C including 95% confidence bounds (dotted lines) to illustrate the error in the probability.

H) Cumulative probability density plots for the measurement of $t_{\text{on stable}}$ for three independent replicates of the *rpoS301* co-transcriptional experiments indicating 95% confidence intervals for each (dotted lines). The co-transcriptional binding replicate experiments have statistically similar kinetics demonstrating repeatability (WT 1 vs WT 2: p = 0.656; WT 1 vs WT 3: p = 0.241; WT 2 vs WT 3: p = 0.699; K-S test).

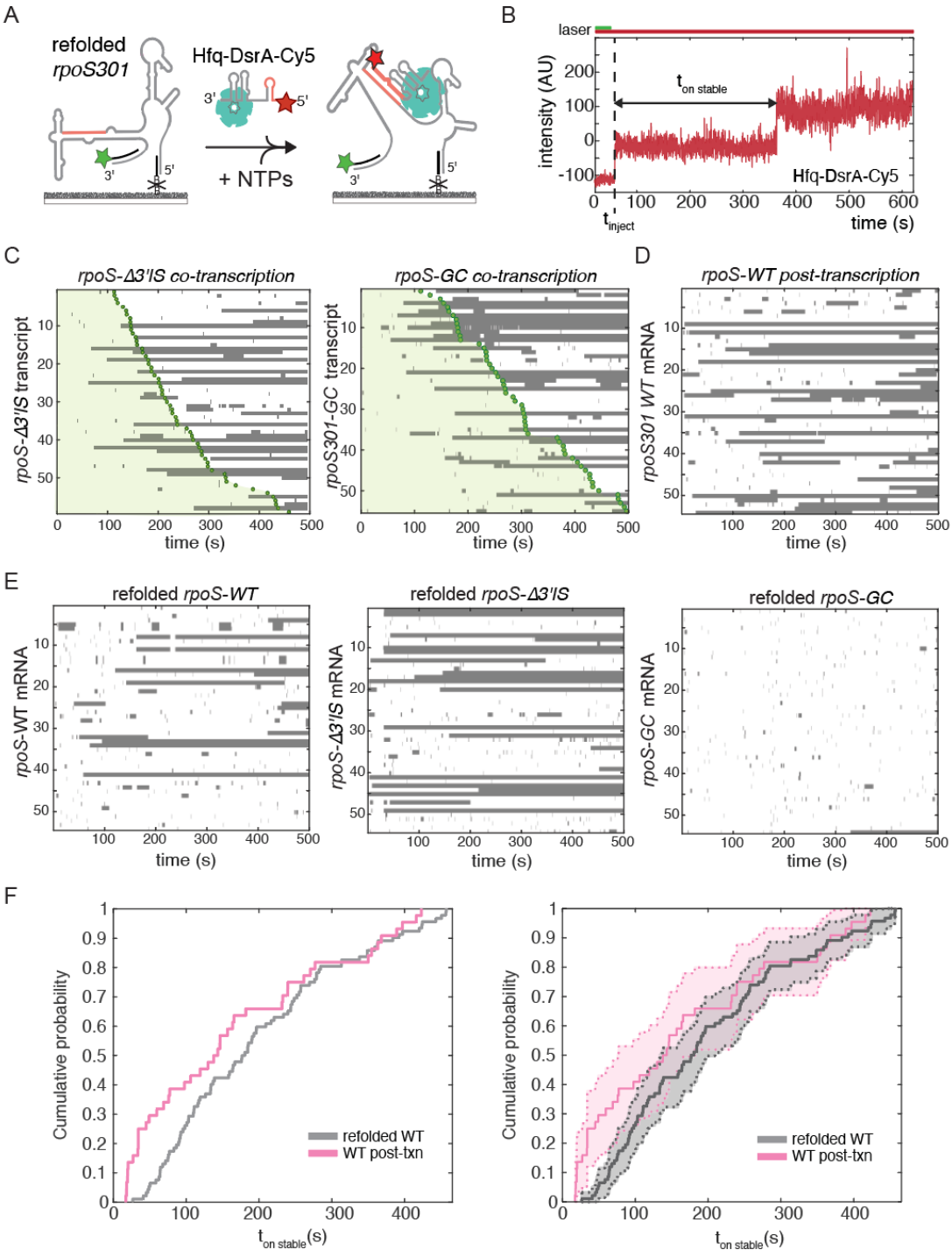

Supplemental Figure S3. Stability of the inhibitory stem affects Hfq-DsrA binding to renatured *rpoS* RNAs and nascent *rpoS* RNAs during transcription. Related to Figure 3.

A) Single-molecule colocalization experiment for monitoring post-transcriptional association of Hfq•DsrA-Cy5 to refolded, full-length *rpoS301* mRNAs. Refolded mRNA was hybridized with a Cy3-labeled anti-sense oligomer (green star) prior to immobilization on the slide.

B) Example time trace for a single refolded *rpoS301* mRNA molecule showing the Hfq•DsrA-Cy5 binding interval, Δt, relative to injection.

C) Rastergrams of Hfq•DsrA-Cy5 binding during transcription to *rpoS301*$\Delta_{3'IS}$ transcripts (left) and *rpoS301*$_{GC}$ transcripts (right). Colored as in Fig. 1. Rastergrams were assembled from 52-55 randomly selected transcripts from a total combined dataset of > 100 total transcripts from at least two independent replicate experiments. The time axis was synchronized with the start of injection (t = 0) for each transcript.

D) Rastergram of Hfq•DsrA-Cy5 binding to WT *rpoS301* mRNA 45 min post-transcription. Rastergrams were assembled as in (C).

E) Rastergrams of Hfq•DsrA-Cy5 binding to refolded mRNAs: *rpoS301 WT* (right), *rpoS301*$\Delta_{3'IS}$ (middle), and *rpoS301*$_{GC}$ (left).

F) Cumulative probability density illustrating the onset of stable Hfq•DsrA binding to refolded WT *rpoS* mRNA and co-transcriptionally folded *rpoS* mRNAs 45 minutes after addition of NTPs to the slide surface (WT post-txn). Above 100 s, the distributions lie within overlapping 95% confidence intervals (right). Before 100 s, excess binding of Hfq-DsrA to the co-transcriptionally folded RNA compared to refolded RNA indicates that a fraction of transcripts remain poorly folded 45 min after transcription and are readily targeted by DsrA.

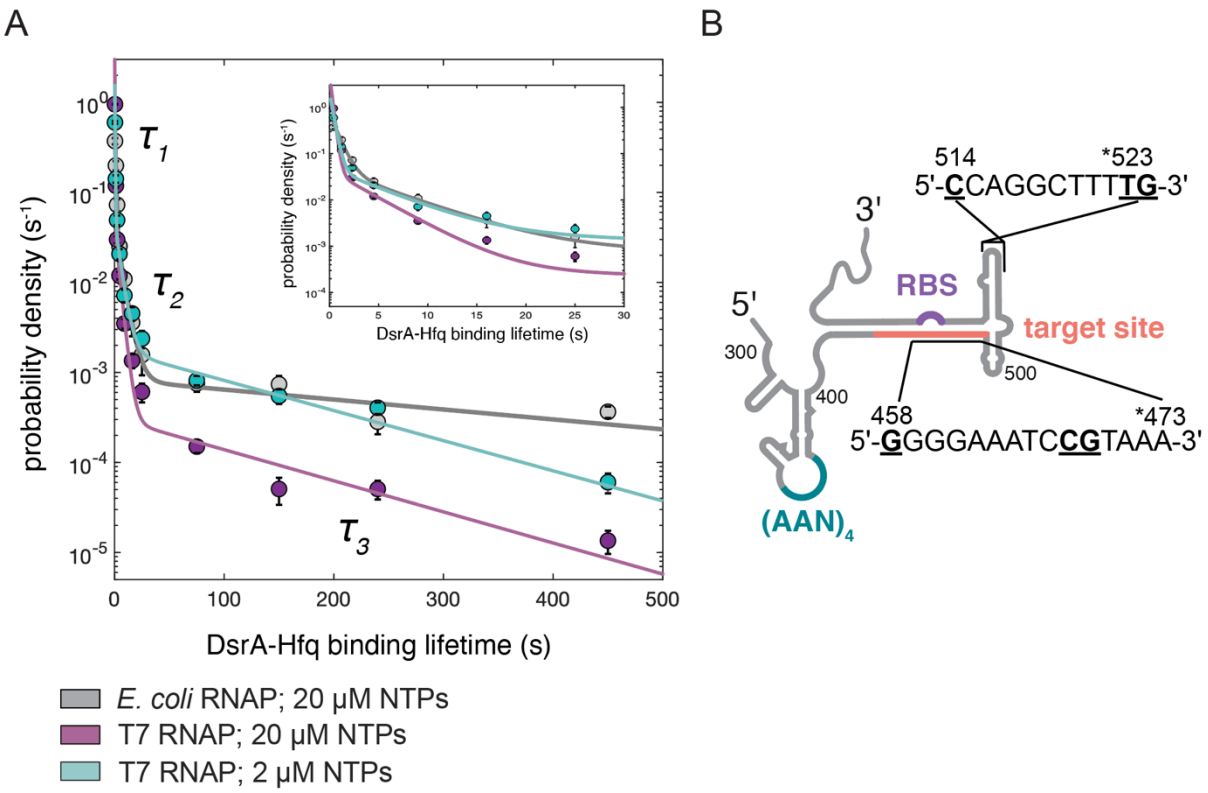

Supplemental Figure S4. Transcription speed influences the likelihood of stable Hfq•DsrA binding. Related to Figure 4.

A) Probability density histogram with overlayed maximum likelihood triple exponential fit illustrating the distribution of DsrA lifetimes for each transcription condition. Faster transcription by T7 RNAP in 20 μM NTPs (purple) reduces the likelihood of forming a stable complex. Equations for fitting can be found in Star Methods. Fit parameters for *rpoS301* mRNA transcribed by *E. coli* RNAP at 20 μM NTPs can be found in Table S1. Fit parameters for T7 RNAP are as follows:

20 μM NTPs: $\tau_1 = 0.24 \pm 0.01$, $\tau_2 = 3.65 \pm 0.5$, $\tau_3 = 126 \pm 19$, $a_1 = 0.86 \pm 0.01$, $a_2 = 0.11 \pm 0.01$, $a_3 = 0.03 \pm 0.01$;

2 μM: $\tau_1 = 0.36 \pm 0.03$, $\tau_2 = 4.9 \pm 1.4$, $\tau_3 = 130 \pm 11$, $a_1 = 0.62 \pm 0.02$, $a_2 = 0.19 \pm 0.01$, $a_3 = 0.19 \pm 0.02$

B) Secondary structure of *rpoS*301 with sequences around observed *in vitro* pause sites. A consensus pause sequence [2] can be found near these mapped sites suggesting these may be used *in vivo*.

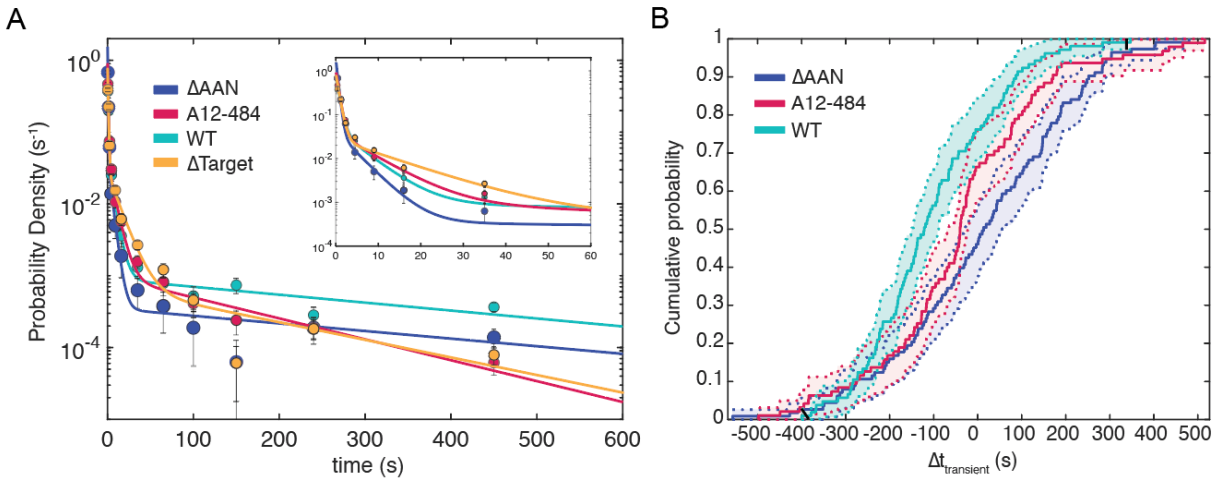

Supplemental Figure S5. Hfq binds transiently to AAN motif during transcription. Related to Figure 5.

A) Probability density histogram with overlayed maximum likelihood triple exponential fit illustrating the distribution of DsrA lifetimes for *rpoS*301 variants lacking an Hfq binding site (ΔAAN), a downstream Hfq binding site (A12-484), or the DsrA binding site (ΔTarget). Inset shows that the probability of forming short-lived complexes (τ_2) is greatest when Hfq can bind an AAN motif but DsrA cannot base pair with the target. Equations for fitting can be found in Star Methods. Fit parameters for each *rpoS*301 variant can be found in Table S1.

B) Cumulative probability density plot as in Figure 5F showing 95% confidence bounds for each variant. $DsrA_{RBM}$ was omitted for clarity and is statistically similar to *rpoS*301 WT (p = 0.888; K-S test).

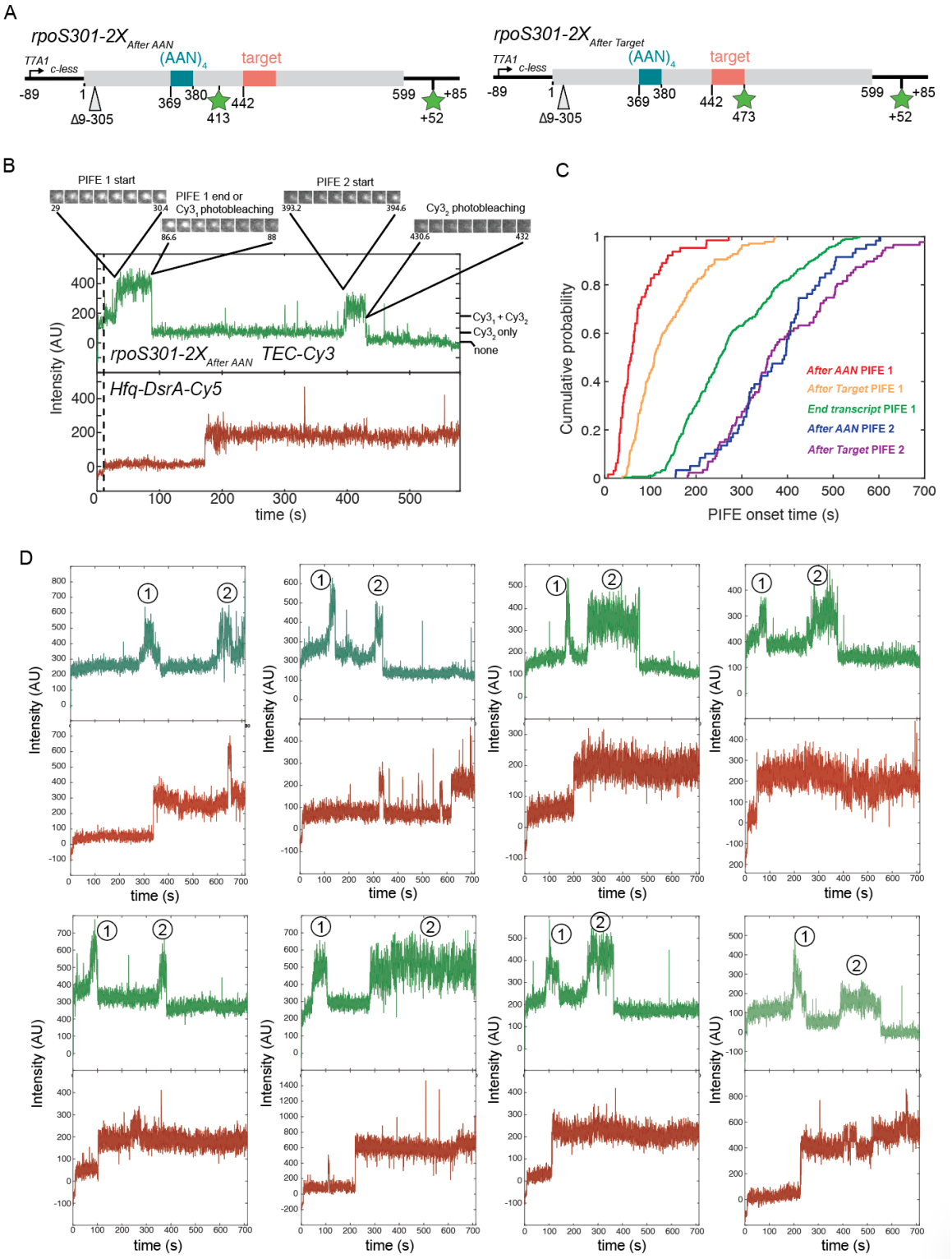

Supplemental Figure S6. PIFE monitors the progress of active transcription. Related to Figure 6.

A) Schematic of doubly labeled DNA templates indicating the positions of Cy3 fluorophores relative to the Hfq binding motif (AAN) and DsrA target site.

B) Example single molecule trajectory illustrating the detection of double PIFE events based on Cy3 fluorescence intensity (green line). (top) Single frame images of the Cy3 fluorescence indicating increased fluorescence observed for one or two Cy3 fluorophores during PIFE 1 and PIFE 2. Notches at the right of the trace indicate the standard intensities of 0, 1, 2 active Cy3 fluorophores. DsrA binding is indicated by an increase in Cy5 intensity (red line).

C) A cumulative probability density plot illustrating the relative timing for the start of PIFE 1 and PIFE 2 for the 2X-*Cy3 labeled rpoS* DNAs (after AAN and after Target shown in part A) compared to PIFE from a singly labeled DNA template with Cy3 located at 599+52 (green), as in Fig. 1C. A significant delay in the onset of PIFE 1 is observed when the Cy3 is incorporated at position 473 (after target, orange) relative to position 413 (after AAN, red), demonstrating that the appearance of PIFE reflects the distance traveled by RNAP before reaching the fluorophore. The cumulative probability density for PIFE 2 becomes similar for both 2X-*Cy3 labeled rpoS* DNAs (blue and purple) because the Cy3 fluorophore is located on the same nucleotide (599+52) in each template. This occurs later than PIFE on a single-labeled DNA template (green) containing Cy3 at the same position (599+52), suggesting the upstream fluorophore impedes elongation to some degree. This effect is the same for both doubly labeled templates and is not sequence specific. This delay in reaching the second fluorophore does not affect the analysis of Hfq•DsrA binding relative to the first PIFE signal.

D) Example single molecule traces of Hfq•DsrA binding relative to elongation of 2x-Cy3-$rpoS_{afterTarget}$. Fluorescence intensity from Cy3 fluorophores located on the 2x-Cy3-$rpoS_{afterTarget}$ DNA template is shown in the top trace (green) and intensity from a Cy5 fluorophore on the 5' end of DsrA sRNA is shown in the bottom trace (red). Numbers indicate first and second PIFE signals from $Cy3_1$ and $Cy3_2$ respectively.

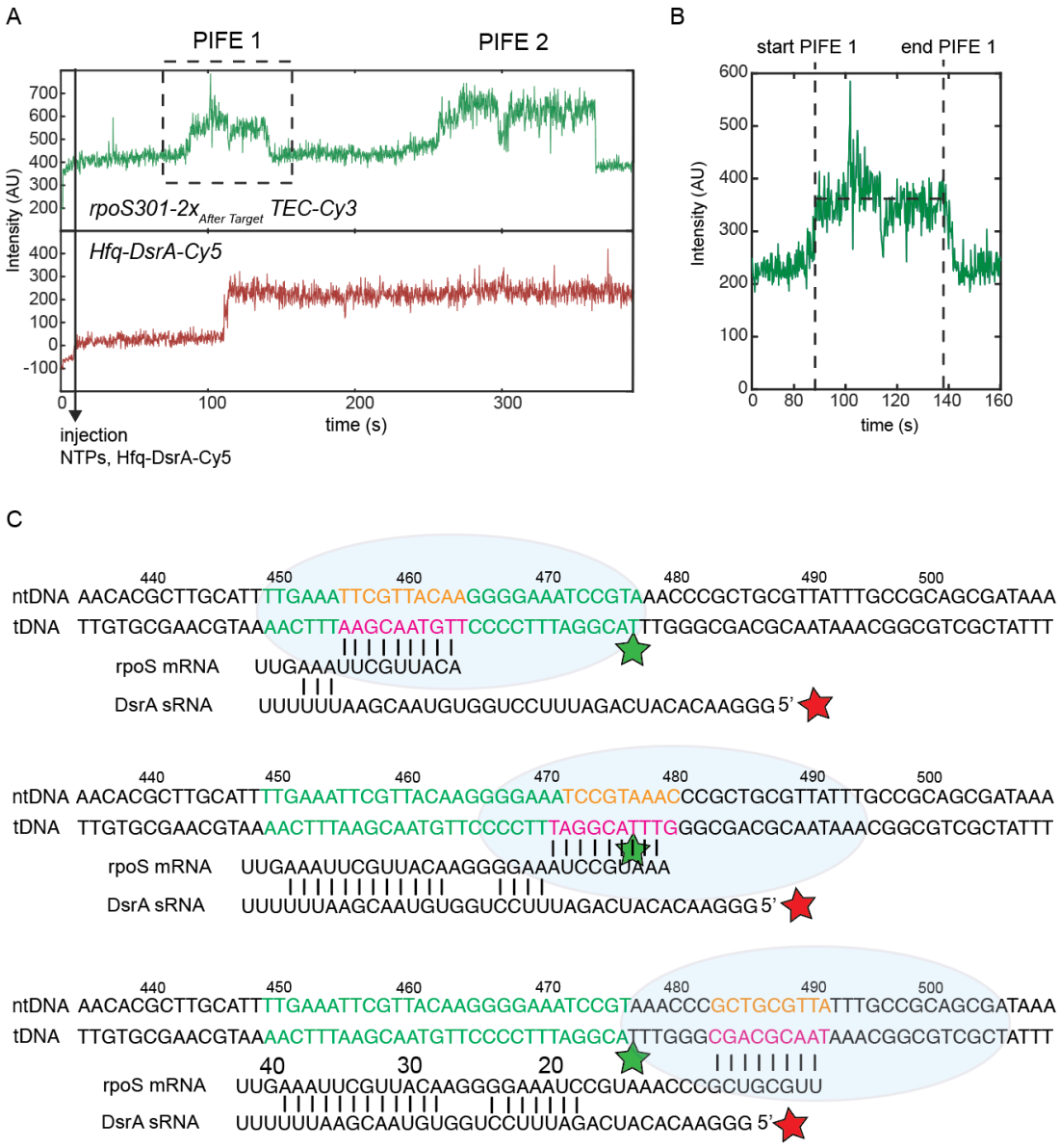

Supplemental Figure S7. Interpretation of the start and end of PIFE signals. Related to Figure 6.

A) Single molecule trace for transcription on 2x-Cy3-*rpoS*$_{\text{afterTarget}}$ DNA (green, top) and DsrA-Cy5 (red, bottom).

B) Expansion of first PIFE signal shown in A, illustrating the identification of the start time and end time from the duration of the PIFE signal plateau (dotted lines). A gradual increase in Cy3 intensity can be seen until the signal reaches the plateau before the start of PIFE 1 and after the end of PIFE 1. Based on the single nanometer distance dependence of PIFE [3–5], we interpret the gradual increase as RNAP approaching the Cy3 fluorophore and the plateau in the PIFE signal as confinement of the Cy3 fluorophore within the active site of *E. coli* RNAP during translocation of the template strand (see also Figure 6G).

C) Map of DsrA target site in *rpoS* mRNA (green letters), relative to the TEC at various stages of *rpoS* transcription. In the structure of the *E. coli* RNAP elongation complex [6], template nucleobases –15 to +14 relative to the insertion site are highly ordered and within 1 – 2 nm of protein residues. Therefore, a Cy3 fluorophore attached to a nucleobase within this 29 bp window would experience an environment conducive to PIFE. We estimate that the PIFE plateau begins when the $Cy3_1$ fluorophore is located on the +14 position in the RNAP active site (top). During the plateau signal, the $Cy3_1$ fluorophore traverses through nucleotide –15 in the template strand before the signal starts to gradually decrease as polymerase moves away from the fluorophore (bottom). Potential base pairing with the DsrA-Cy5 sRNA is shown on the nascent *rpoS301* mRNA for each scenario, assuming DsrA can extend into the exit channel up to 1 nt behind the DNA-RNA hybrid (magenta). This extent of base pairing is consistent with recent structures of *E. coli* termination complexes. [7–9]

Supplemental Tables

Table S1. Characteristic lifetimes of Hfq•DsrA•*rpoS* mRNA complexes.[a] Related to Figures 2, 3, and 5.

Experiment	N_{mol}[b]	N_{events}[b]	τ_1 (s)	τ_2 (s)	τ_3 (s)	a_1	a_2	a_3
Hfq•DsrA + *rpoS301*	199	383	0.8 ± 0.1	5.7 ± 2.2	393 ± 73	0.46 ± 0.05	0.23 ± 0.01	0.31 ± 0.05
DsrA alone + *rpoS301*	208	265	0.6 ± 0.1	5.2 ± 3.6	120 ± 93	0.78 ± 0.14	0.16 ± 0.01	0.06 ± 0.14
Hfq•$DsrA_{RBM}$ + *rpoS301*	114	382	0.3 ± 0.1	5.5 ± 1.6	62 ± 20	0.65 ± 0.03	0.26 ± 0.02	0.09 ± 0.04
Hfq•DsrA + refolded *rpoS301*	246	870	0.8 ± 0.1	7.5 ± 1.3	303 ± 66	0.62 ± 0.03	0.21 ± 0.01	0.17 ± 0.03
Hfq•DsrA + $rpoS301_{GC}$	150	583	0.59 ± 0.8	5.8 ± 3.3	185 ± 74	0.61 ± 0.04	0.21 ± 0.02	0.18 ± 0.04
Hfq•DsrA + $rpoS301\Delta_{3'IS}$	101	380	0.49 ± 0.7	11.0 ± 3.4	253 ± 131	0.61 ± 0.03	0.23 ± 0.01	0.16 ± 0.03
Hfq•DsrA + $rpoS301\Delta_{AAN}$	208	265	0.47 ± 0.8	4.4 ± 2.7	410 ± 114	0.73 ± 0.1	0.15 ± 0.01	0.12 ± 0.1
Hfq•DsrA + $rpoS301_{A12\text{-}484}$	120	486	0.67 ± 0.1	7.4 ± 2.4	149 ± 72	0.61 ± 0.03	0.26 ± 0.02	0.13 ± 0.04
Hfq•DsrA + $rpoS301\Delta_{target}$	153	549	0.74 ± 0.8	12.9 ± 3.9	177 ± 87	0.57 ± 0.04	0.32 ± 0.02	0.11 ± 0.04

[a]Equations for maximum likelihood estimates are described in Methods. All experiments shown include data combined from 2 independent trials. Errors are taken from bootstrapping of the data as described in Methods. Lifetimes (τ_1, τ_2, τ_3) correspond to transient, short-lived, and stable binding events described in the text. Their corresponding amplitudes (a_1, a_2, a_3) represent the likelihood of a complex with that lifetime occurring among all events analyzed.

[b]Number of distinct TEC molecules (N_{mol}) and total number of binding events (N_{events}) used in each analysis.

Table S2. Fraction of *rpoS* mRNA with stable Hfq•DsrA binding. Related to Figures 2 – 5.

Experiment	Replicate[a]	N_{mol}[a]	fraction[b]
Hfq•DsrA + *rpoS301*	1	85	0.435
Hfq•DsrA + *rpoS301*	2	96	0.510
DsrA alone + *rpoS301*	1	115	0.017
DsrA alone + *rpoS301*	2	93	0.022
Hfq•$DsrA_{RBM}$ + *rpoS301*	1	110	0.127
Hfq•$DsrA_{RBM}$ + *rpoS301*	2	114	0.044
Hfq•DsrA + refolded *rpoS301*	1	177	0.254
Hfq•DsrA + refolded *rpoS301*	2	106	0.387
Hfq•DsrA + refolded *rpoS301*	3	103	0.262
Hfq•DsrA + *rpoS301$_{GC}$ co-txn*	1	65	0.554
Hfq•DsrA + *rpoS301$_{GC}$* co-txn	2	85	0.310
Hfq•DsrA + *rpoS301$_{GC}$* co-txn	3	35	0.4
Hfq•DsrA + refolded *rpoS301$_{GC}$*	1	134	0.112
Hfq•DsrA + refolded *rpoS301$_{GC}$*	2	101	0.020
Hfq•DsrA + refolded *rpoS301$_{GC}$*	3	99	0.010
Hfq•DsrA + *rpoS301Δ$_{3'IS}$* co-txn	1	59	0.441
Hfq•DsrA + *rpoS301Δ$_{3'IS}$* co-txn	2	42	0.476
Hfq•DsrA + refolded *rpoS301Δ$_{3'IS}$*	1	101	0.257
Hfq•DsrA + refolded *rpoS301Δ$_{3'IS}$*	2	99	0.376
Hfq•DsrA + *rpoS301Δ$_{AAN}$*	1	103	0.078
Hfq•DsrA + *rpoS301Δ$_{AAN}$*	2	105	0.105
Hfq•DsrA + *rpoS301$_{A12-484}$*	1	49	0.143
Hfq•DsrA + *rpoS301$_{A12-484}$*	2	71	0.127
Hfq•DsrA + *rpoS301Δ$_{target}$*	1	101	0.188
Hfq•DsrA + *rpoS301Δ$_{target}$*	2	103	0.282
Hfq•DsrA + *rpoS301* T7 RNAP 20 μM NTPs	1	81	0.259
Hfq•DsrA + *rpoS301* T7 RNAP 20 μM NTPs	2	82	0.097
Hfq•DsrA + *rpoS301* T7 RNAP 20 μM NTPs	3	111	0.225
Hfq•DsrA + *rpoS301* T7 RNAP 2 μM NTPs	1	94	0.478
Hfq•DsrA + *rpoS301* T7 RNAP 2 μM NTPs	2	102	0.353
Hfq•DsrA + *rpoS301* T7 RNAP 2 μM NTPs	3	44	0.409

[a]Number of distinct TEC molecules (N_{mol}) used in each analysis.

[b]Fraction of TEC molecules that formed a stable complex with DsrA (t > 100 s) during the 10 min movie.

Table S3. Sequences for DNA transcription templates[a]. Related to STAR Methods.

rpoS full	TATCAAAAAGAGTATTGACTTAAAGTCTAACCTATAGGATACTTACAGCCAGGTGAGTGAGAG ATGGATGGGTAGAGAGTTAGTAGTAAGGGTGAACAGAGTGCTAACAAAATGTTGCCGAACAA CAAGCCAACTGCGACCACGGTCACAGCGCCTGTAACGGTACCAACAGCAAGCACAACCGAG CCGACTGTCAGCAGTACATCAACCAGTACGCCTATCTCCACCTGGCGCTGGCCGACTGAGG GCAAAGTGATCGAAACCTTTGGCGCTTCTGAGGGGGGCAACAAGGGGATTGATATCGCAGG CAGCAAAGGACAGGCAATTATCGCGACCGCAGATGGCCGCGTTGTTTATGCTGGTAACGCG CTGCGCGGCTACGGTAATCTGATTATCATCAAACATAATGATGATTACCTGAGTGCCTACGC CCATAACGACACAATGCTGGTCCGGGAACAACAAGAAGTTAAGGCGGGGCAAAAAATAGCG ACCATGGGTAGCACCGGAACCAGTTCAACACGCTTGCATTTTGAAATTCGTTACAAGGGGAA ATCCGTAAACCCGCTGCGTTATTTGCCGCAGCGATAAATCGGCGGAACCAGGCTTTTGCTTG AATGTTCCGTCAAGGGATCACGGGTAGGAGCCACCTTATGAGTCAGAATACGCTGAAAGTTC ATGATGGACGACACACTTTGGACAGGACACACAGGACACAGGCTAGCATAACCCCTTGGGG CCTCTAAACGGGTCTTGAGGGGTTTTTTG
rpoS301	TATCAAAAAGAGTATTGACTTAAAGTCTAACCTATAGGATACTTACAGCCAGGTGAGTGAGAG ATGGATGGGTAGAGAGTTAGTAGTAAGGGTGAACGATTATCATCAAACATAATGATGATTAC CTGAGTGCCTACGCCCATAACGACACAATGCTGGTCCGGGAACAACAAGAAGTTAAGGCGG GGCAAAAAATAGCGACCATGGGTAGCACCGGAACCAGTTCAACACGCTTGCATTTTGAAATT CGTTACAAGGGGAAATCCGTAAACCCGCTGCGTTATTTGCCGCAGCGATAAATCGGCGGAA CCAGGCTTTTGCTTGAATGTTCCGTCAAGGGATCACGGGTAGGAGCCACCTTATGAGTCAGA ATACGCTGAAAGTTCATGATGGACGACACACTTTGGACAGGACACACAGGACACAGGCTAG CATAACCCCTTGGGGCCTCTAAACGGGTCTTGAGGGGTTTTTTG
rpoS301 T7 RNAP	GCTCGGTACCCGGGGATCCTAATACGACTCACTATAGGGTGAGTGAGAGATGGATGGGTAG AGAGTTAGTAGTAAGGGTGAACGATTATCATCAAACATAATGATGATTACCTGAGTGCCTACG CCCATAACGACACAATGCTGGTCCGGGAACAACAAGAAGTTAAGGCGGGGCAAAAAATAGC GACCATGGGTAGCACCGGAACCAGTTCAACACGCTTGCATTTTGAAATTCGTTACAAGGGGA AATCCGTAAACCCGCTGCGTTATTTGCCGCAGCGATAAATCGGCGGAACCAGGCTTTTGCTT GAATGTTCCGTCAAGGGATCACGGGTAGGAGCCACCTTATGAGTCAGAATACGCTGAAAGTT CATGATGGACGACACACTTTGGACAGGACACACAGGACACAGGCTAGCATAACCCCTTGGG GCCTCTAAACGGGTCTTGAGGGGTTTTTTG
rpoS301 ΔAAN	TATCAAAAAGAGTATTGACTTAAAGTCTAACCTATAGGATACTTACAGCCAGGTGAGTGAGAG ATGGATGGGTAGAGAGTTAGTAGTAAGGGTGAACGATTATCATCAAACATAATGATGATTAC CTGAGTGCCTACGCCCATAACGACACAATGCTGGTCCGGGGAGCATCTAGGCGTTAAGGCGG GGCACGTGATAGCGACCATGGGTAGCACCGGAACCAGTTCAACACGCTTGCATTTTGAAATT CGTTACAAGGGGAAATCCGTAAACCCGCTGCGTTATTTGCCGCAGCGATAAATCGGCGGAA CCAGGCTTTTGCTTGAATGTTCCGTCAAGGGATCACGGGTAGGAGCCACCTTATGAGTCAGA ATACGCTGAAAGTTCATGATGGACGACACACTTTGGACAGGACACACAGGACACAGGCTAG CATAACCCCTTGGGGCCTCTAAACGGGTCTTGAGGGGTTTTTTG
rpoS301 A12-484	TATCAAAAAGAGTATTGACTTAAAGTCTAACCTATAGGATACTTACAGCCAGGTGAGTGAGAG ATGGATGGGTAGAGAGTTAGTAGTAAGGGTGAACGATTATCATCAAACATAATGATGATTAC CTGAGTGCCTACGCCCATAACGACACAATGCTGGTCCGGGGAGCATCTAGGCGTTAAGGCGG GGCACGTGATAGCGACCATGGGTAGCACCGGAACCAGTTCAACACGCTTGCATTTTGAAATT CGTTACAAGGGGAAATCCGTAAACCCGCTGCGTTATTAAAAAAAAAAAATGCCGCAGCGATA AATCGGCGGAACCAGGCTTTTGCTTGAATGTTCCGTCAAGGGATCACGGGTAGGAGCCACC TTATGAGTCAGAATACGCTGAAAGTTCATGATGGACGACACACTTTGGACAGGACACACAGG ACACAGGCTAGCATAACCCCTTGGGGCCTCTAAACGGGTCTTGAGGGGTTTTTTG
rpoS301 ΔTarget	TATCAAAAAGAGTATTGACTTAAAGTCTAACCTATAGGATACTTACAGCCAGGTGAGTGAGAG ATGGATGGGTAGAGAGTTAGTAGTAAGGGTGAACGATTATCATCAAACATAATGATGATTAC CTGAGTGCCTACGCCCATAACGACACAATGCTGGTCCGGGAACAACAAGAAGTTAAGGCGG GGCAAAAAATAGCGACCATGGGTAGCACCGGAACCAGTTCAACACGCTTGCAGGACGACAC ACTTTGGACAGGACACACAGGACACAGGCTAGCATAACCCCTTGGGGCCTCTAAACGGGTC TTGAGGGGTTTTTTG
rpoS301 GC clamp	TATCAAAAAGAGTATTGACTTAAAGTCTAACCTATAGGATACTTACAGCCAGGTGAGTGAGAG ATGGATGGGTAGAGAGTTAGTAGTAAGGGTGAACGATTATCATCAAACATAATGATGATTAC CTGAGTGCCTACGCCCATAACGACACAATGCTGGTCCGGGAACAACAAGAAGTTAAGGCGG GGCAAAAAATAGCGACCATGGGTAGCACCGGAACCAGTTCAACACGCTTGCAGGGGGAAAT TCGTTACAAGGGGAAATCCGTAAACCCGCTGCGTTATTTGCCGCAGCGATAAATCGGCGGA ACCAGGCTTTTGCTTGAATGTTCCGTCAAGGGATCACGGGTAGGAGCCACCTTATGAGTCCC CATACGCTGAAAGTTCATGATGGACGACACACTTTGGACAGGACACACAGGACACAGGCTA GCATAACCCCTTGGGGCCTCTAAACGGGTCTTGAGGGGTTTTTTG

rpoS301 Δ3' IS	TATCAAAAAGAGTATTGACTTAAAGTCTAACCTATAGGATACTTACAGCCAGGTGAGTGAGAG ATGGATGGGTAGAGAGTTAGTAGTAAGGGTGAACGATTATCATCAAACATAATGATGATTAC CTGAGTGCCTACGCCCATAACGACACAATGCTGGTCCGGGAACAACAAGAAGTTAAGGCGG GGCAAAAAATAGCGACCATGGGTAGCACCGGAACCAGTTCAACACGCTTGCATTTTGAAATT CGTTACAAGGGGAAATCCGTAAACCCGCTGCGTTATTTGCCGCAGCGATAAATCGGCGGAA CCAGGCTTTTGCTTGAATGTTCCGTCGGACGACACACTTTGGACAGGACACACAGGACACA GGCTAGCATAACCCCTTGGGGCCTCTAAACGGGTCTTGAGGGGTTTTTTG
rpoS301 2X-Cy3$_{afterAAN}$	TATCAAAAAGAGTATTGACTTAAAGTCTAACCTATAGGATACTTACAGCCAGGTGAGTGAGAG ATGGATGGGTAGAGAGTTAGTAGTAAGGGTGAACGATTATCATCAAACATAATGATGATTAC CTGAGTGCCTACGCCCATAACGACACAATGCTGGTCCGGGAACAACAAGAAGTTAAGGCGG GGCAAAAAATAGCGACCATGGGTAGCACCGGAACCAGTTCAACACGCTTGCATTTTGAAATT CGTTACAAGGGGAAATCCGTAAACCCGCTGCGTTATTTGCCGCAGCGATAAATCGGCGGAA CCAGGCTTTTGCTTGAATGTTCCGTCAAGGGATCACGGGTAGGAGCCACCTTATGAGTCAGA ATACGCTGAAAGTTCATGATGGACGACACACTTTGGACAGGACACACAGGACACAGGCTAG CATAACCCCTTGGGGCCTCTAAACGGGTCTTGAGGGGTTTTTTG
rpoS301 2X-Cy3$_{afterTarget}$	TATCAAAAAGAGTATTGACTTAAAGTCTAACCTATAGGATACTTACAGCCAGGTGAGTGAGAG ATGGATGGGTAGAGAGTTAGTAGTAAGGGTGAACGATTATCATCAAACATAATGATGATTAC CTGAGTGCCTACGCCCATAACGACACAATGCTGGTCCGGGAACAACAAGAAGTTAAGGCGG GGCAAAAAATAGCGACCATGGGTAGCACCGGAACCAGTTCAACACGCTTGCATTTTGAAATT CGTTACAAGGGGAAATCCGTAAACCCGCTGCGTTATTTGCCGCAGCGATAAATCGGCGGAA CCAGGCTTTTGCTTGAATGTTCCGTCAAGGGATCACGGGTAGGAGCCACCTTATGAGTCAGA ATACGCTGAAAGTTCATGATGGACGACACACTTTGGACAGGACACACAGGACACAGGCTAG CATAACCCCTTGGGGCCTCTAAACGGGTCTTGAGGGGTTTTTTG

[a]Sequence of the coding (non-template) strand is shown (5′ to 3′). Highlighted colors indicate features of the DNA template design: Transcription restart (underscore), $(AAN)_4$ Hfq binding motif (magenta), DsrA annealing target (cyan), mutated region (red), A12 insertion (yellow), Cy3 fluorophore placement on template strand (green).

Supplemental References:

1. Soper, T.J., Doxzen, K., Woodson, S.A. (2011). Major role for mRNA binding and restructuring in sRNA recruitment by Hfq. RNA 17, 1544–1550.

2. Larson, M.H., Mooney, R.A., Peters, J.M., Windgassen, T., Nayak, D., Gross, C.A., Block, S.M., Greenleaf, W.J., Landick, R., Weissman, J.S. (2014). A pause sequence enriched at translation start sites drives transcription dynamics in vivo. Science 344, 1042 1047.

3. Hwang, H., Myong, S. (2014). Protein induced fluorescence enhancement (PIFE) for probing protein-nucleic acid interactions. Chem Soc Rev. 43, 1221–1229.

4. Lerner, E., Ploetz, E., Hohlbein, J., Cordes, T., Weiss, S. A. (2016). Quantitative theoretical framework for protein-induced fluorescence enhancement–Förster-type resonance energy transfer (PIFE-FRET). J Phys Chem B. 120, 6401–6410.

5. Ploetz, E., Lerner, E., Husada, F., Roelfs, M., Chung, S., Hohlbein, J., Weiss, S., Cordes, T. (2016). Förster resonance energy transfer and protein-induced fluorescence enhancement as synergetic multi-scale molecular rulers. Sci Rep 6, 33257.

6. Kang, J.Y., Olinares, P.D.B., Chen, J., Campbell, E.A., Mustaev, A., Chait, B.T., Gottesman, M.E., Darst, S.A. (2017). Structural basis of transcription arrest by coliphage HK022 Nun in an Escherichia coli RNA polymerase elongation complex. Elife 6, e25478.

7. You, L., Omollo, E.O., Yu, C., Mooney, R.A., Shi, J., Shen, L., Wu, X., Wen, A., He, D., Zeng, Y., Feng, Y., Landick, R., Zhang, Y. (2023). Structural basis for intrinsic transcription termination. Nature 613, 783–789.

8. Molodtsov, V., Wang, C., Firlar, E., Kaelber, J.T., Ebright, R.H. (2023). Structural basis of Rho-dependent transcription termination. Nature 614, 367-374.

9. Said, N., Hilal, T., Sunday, N.D., Khatri, A. ,Bürger, J., Mielke, T., Belogurov, G.A., Loll, B., Sen, R., Artsimovitch, I., Wahl, M.C. (2021). Steps toward translocation-independent RNA polymerase inactivation by terminator ATPase ρ. Science 371, eabd1673.